Characteristics of the Complex Received Signal in Dynamic Body Area Networks

Simon L. Cotton[1], Arjan Meijerink[2] and William G. Scanlon[1,2]
[1]ECIT Institute, Queen's University, Belfast, UK, {simon.cotton, w.scanlon}@qub.ac.uk
[2]Telecommunication Engineering Group, University of Twente, The Netherlands, a.meijerink@utwente.nl

Abstract—**This paper investigates the characteristics of the complex received signal in body area networks for two environments at the opposite ends of the multipath spectrum at 2.45 GHz. Important attributes of the complex channel such as the Gaussianity of the quadrature components and power imbalance, which form the basis of many popular fading models, are investigated. It is found that in anechoic environments the assumption of Gaussian distributed quadrature components will not always yield a satisfactory fit. Using a complex received signal model which considers a non-isotropic scattered signal contribution along with the presence of an optional dominant signal component, we use an autocorrelation function originally derived for mobile-to-mobile communications to model the temporal behavior of a range of dynamic body area network channels with considerable success. In reverberant environments, it was observed that the real part of the complex autocorrelation function for body area network channels decayed slightly quicker than that expected in traditional land mobile channels.**

I. INTRODUCTION

Our knowledge of the characteristics of signal propagation in body area networks (BANs) has improved considerably over the last decade. Strong contributions have been made to the modeling of signal reception in both narrowband [1-4] and ultra-wideband BAN [5] systems. For narrowband BANs many different fading models such as Lognormal [1], Rice [2], Nakagami [3] and Weibull [3, 4] have been proposed to describe the variation of the received signal. While there is some discussion on the statistics of the fading model most suited to BAN communications, one thing that is prevalent in many of these studies is that human body movement and the characteristics of the local environment are important factors in determining not only the statistical distribution of the fading but also its variation in time.

Due to the often repetitive nature of human body movement caused by both physiological and biomechanical processes, it is anticipated and indeed expected that noticeable correlation may exist between current and previous observations of the received signal [6]. A function that is useful for determining the variation of a stochastic processes is the autocorrelation function (ACF). At present our understanding of the autocorrelation in body area networks is somewhat limited. In [4] a Weibull correlation function was fitted to the amplitude data for a number of on-body channels assuming isotropic signal reception. The authors averaged a number of distinct on-body channels for walking and running scenarios and showed that the Weibull ACF best described the temporal data. In [6] autoregressive models were constructed after considering the autocorrelation statistics of the fading amplitude in BANs. Here the autocorrelation and cross-correlation functions were shown to be dependent on body state and surroundings.

In this paper we consider a very general complex ACF developed for mobile-to-mobile communications [7]. In this model signal transmission and reception can be non-isotropic and subject to an optional dominant component which predominates over the scattered signal contribution. At first it might seem unusual that models developed for mobile-to-mobile communications could be applied to the study of signal propagation in BANs. However, although the signal propagation paths connecting on-body nodes are considerably shorter than traditional mobile-to-mobile communications, BANs share the characteristics that both ends of the link may be in motion and subject to scattering in both the vicinity of the transmitting and receiving nodes.

The remainder of this paper is organized as follows. In Section II we describe the measurement setup and procedure. The complex signal model used for this study is introduced in Section III. The distribution of the in-phase and quadrature components is also investigated in Section III alongside the estimated power imbalance of the quadrature components. Section IV discusses the use of Von Mises distribution to model the angle of departure (AOD) and angle of arrival (AOA) of the transmitted signal in BANs. The complex autocorrelation function for non-isotropic mobile-to-mobile fading channels is then fitted to the experimental data. Finally, Section V finishes the paper with some concluding remarks.

II. MEASUREMENT SETUP AND PROCEDURE

Two separate measurement environments, namely an anechoic chamber and a reverberation chamber, were chosen. These environments are considered to be representative of the minimum (anechoic) and maximum (reverberation) environmental multipath conditions likely to be experienced by everyday BAN users. To facilitate a study of the complex signal variation solely due to body movements, the mechanical stirrers in the reverberation chamber were disabled. Seven on-body receiver node locations, representative of a BAN, were also selected. These were the head, front chest, waist, knee, ankle, wrist, and elbow all situated on the right side of the user's body. As shown in Fig. 1, the transmitter was located at the user's left waist. This setup ensured that all on-body links were in non-line of sight (LOS) and that any dominant

978-1-4577-1348-4/13/$31.00 ©2013 IEEE

component observed in the results was not due to free space propagation.

The antennas used in this study were compact (5 mm height) higher mode microstrip patch antennas which operate at 2.45 GHz [8]. The test subject was an adult male of height 1.82 m and mass 90 kg. In the experiments, the antennas were mounted so that the radiating patch element was parallel to the body surface and they were connected to a vector network analyzer (Rhode & Schwarz ZVB-8 VNA) using calibrated low-loss coaxial cables. The VNA was configured to record measurements of S_{21} at 5 ms intervals for 30 seconds. For all measurements, the user performed two trials of a walking motion at a set location in both environments. Each of the individual, complex received signal data sets analyzed in this study consisted of 6000 samples, giving a cumulative total of 168000 samples over both experiments.

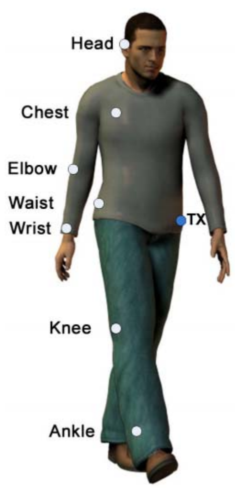

Fig. 1 Wireless nodes on the human body forming a BAN.

III. First Order Statistics of the In-Phase and Quadrature Components

As a starting point for our analysis, we consider the assumption of Gaussian quadrature components which form the basis of many popular fading models such as Hoyt, Rayleigh and Rice. In Ricean fading channels, a dominant signal component exists which predominates over the scattered signal contribution. This situation is often characterized by the Ricean K parameter. The Ricean K parameter is defined as the ratio between the power of the dominant component (s^2) and the total power of the scattered waves ($2\sigma^2$) which may be expressed as $K = s^2/2\sigma^2$ [9].

The distribution of the received signal envelope in a Ricean fading channel can be expressed as in terms of the K parameter as [10]

$$f_R(r) = \frac{2(1+K)r}{\Omega}\exp\left(-K - \frac{(1+K)r^2}{\Omega}\right) \times I_0\left(2\sqrt{\frac{K(K+1)}{\Omega}}r\right),\ r \ge 0,\ K \ge 0,\ \Omega \ge 0 \quad (1)$$

where $I_0(\bullet)$ is the modified Bessel function of the first kind order zero, r is the received signal amplitude and Ω is the mean signal power, $E\left[r^2\right]$, given by $\Omega = s^2 + 2\sigma^2$. As $K \to 0$, and hence the dominant component s decreases, the fading becomes closer to Rayleigh fading, and as $K \to \infty$, the channel no longer exhibits fading.

Now let us define the complex received signal for a Ricean distributed fading channel. Letting $R(t)$ represent the received signal envelope of the Ricean fading process, then $R(t)$ can be expressed in terms of its in-phase and quadrature components as $R(t) = \sqrt{(X+\mu_X)^2 + (Y+\mu_Y)^2}$ where X and Y are mutually independent Gaussian processes with $E[X] = E[Y] = 0$, and μ_X and μ_Y the mean values of the in-phase and quadrature components. Grouping the scattered and dominant components together, for this model, the complex received signal, $z(t)$, can be expressed as

$$z(t) = \frac{\sqrt{\Omega}g(t) + \sqrt{K\Omega}d(t)}{\sqrt{K+1}} \quad (2)$$

where $g(t)$ is the normalized complex received signal due to scattered contributions in the fading channel and $d(t)$ represents the dominant signal component.

To adapt the model given in (2) for use in BAN fading channels, we now use Akki and Haber's model [11] to represent the scattered signal components. Using the notation given in [9, p.82], a mathematical reference model for the scattered component of the normalized flat fading complex received signal may now be written as

$$g(t) = \sqrt{\frac{1}{N}}\sum_{n=1}^{N}\exp\left[j2\pi t\left(f_m^T\cos\theta_n^T + f_m^R\cos\theta_n^R\right) + j\varphi_n\right] \quad (3)$$

where N is the number of propagation paths, f_m^T and f_m^R are the maximum Doppler frequencies at the transmitter and receiver respectively, θ_n^T is the random angle of departure and θ_n^R is the random angle of arrival, of the n^{th} propagation path with reference to the transmitter and receiver velocity vectors respectively. The variable φ_n is a random phase uniformly distributed on $[-\pi,\pi)$ and is independent of θ_n^T and θ_n^R for all n. The dominant component, $d(t)$, can be expressed as $\exp\left[j\left(2\pi f_m^T t\cos(\pi-\theta_d) + 2\pi f_m^R t\cos\theta_d\right)\right]$ where θ_d is the angle of arrival of the specular component [7].

A. Gaussianity

Figs. 2 and 3 show the empirical probability density function (PDF) of the in-phase and quadrature components of the BAN channel for a selection of on-body links in the anechoic chamber. Also shown for comparison are the estimated Gaussian distribution fits (shown as continuous lines). As we can see, the Gaussian distribution provides a reasonable fit for positions such as the wrist. However for some locations such as the knee (worst overall fit) and waist it is less satisfactory.

In the reverberation chamber, due to the additional multipath components generated by the surroundings it was anticipated that the Gaussian PDF would provide an improved fit to the empirical PDF of the quadrature components. Figs. 4 and 5 show the same locations considered above except this time for the reverberation chamber. Compared to the anechoic chamber, the majority of the on-body links were reasonably well approximated by the Gaussian distribution although for positions such as the chest and the knee the Gaussian PDF could not track all the changes in shape of the empirical distribution. The noticeably different shapes and locations of the in-phase and quadrature PDFs obtained for both environments show that the local surroundings are an important factor in determining the characteristics of on-body channels.

B. Power Imbalance

Another useful metric in the analysis of the received complex signal is that of the power imbalance between the quadrature components. Here we express the power imbalance as the ratio, in decibels, of the mean power contribution of the quadrature component to the mean power contribution of the in-phase component i.e.

$$\overline{P}_{imbalance}\left(dB\right) = 10\log_{10}\left(E\left[Q\left(t\right)^{2}\right] \Big/ E\left[I\left(t\right)^{2}\right]\right) \qquad (4)$$

where $I(t)$ and $Q(t)$ represent the signal levels of the in-phase and quadrature components respectively. The mean power imbalance for all of the links considered in this study are shown in Table I. In the anechoic chamber, for the majority of cases the power imbalance was quite low (~0 dB). In this environment, the chest and the knee positioned antennas recorded the greatest power imbalance between the in-phase and quadrature components which were −4.7 dB and −1.7 dB respectively. In the reverberation chamber, the power imbalance was generally lower than that for the anechoic chamber with both the elbow and knee experiencing the greatest imbalance which was less than −1.5 dB.

TABLE I
QUADRATURE COMPONENT POWER IMBALANCE IN DECIBELS

Environment	Ankle	Chest	Elbow	Head	Knee	Waist	Wrist
Anechoic Chamber	−0.1	−4.7	−0.2	−0.1	−1.7	0.6	−0.2
Reverberation Chamber	1.3	0.0	−1.4	0.4	−1.4	0.0	−0.3

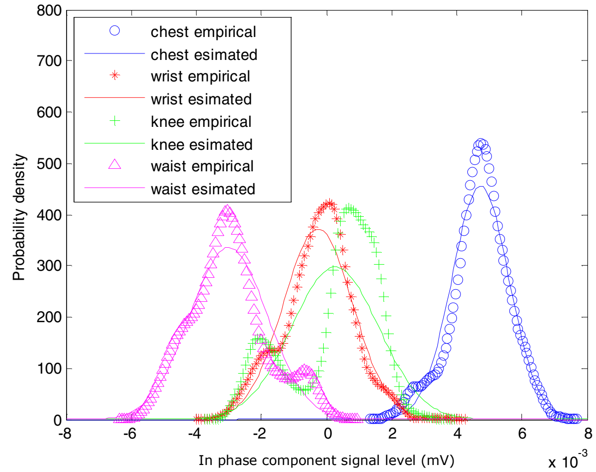

Fig. 2 Empirical and estimated probability densities of the in-phase component for a selection of antenna positions in the anechoic chamber.

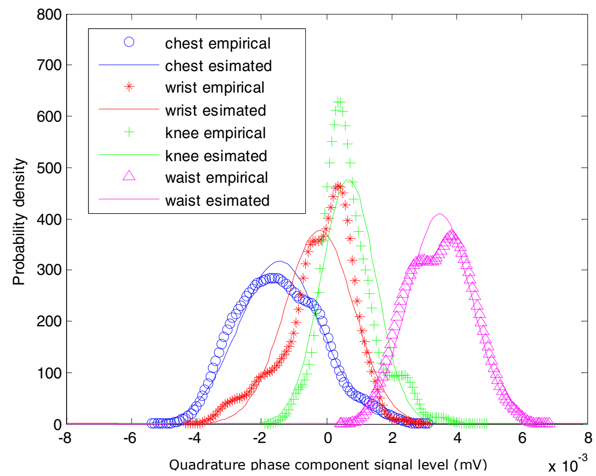

Fig. 3 Empirical and estimated probability densities of the quadrature component for a selection of antenna positions in the anechoic chamber.

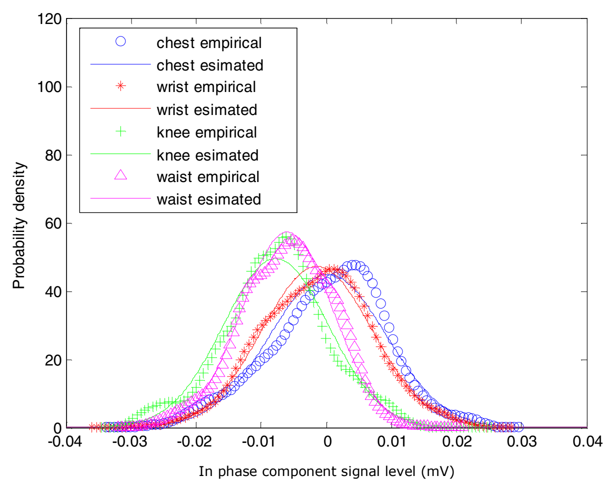

Fig. 4 Empirical and estimated probability densities of the in-phase component for a selection of antenna positions in the reverberation chamber.

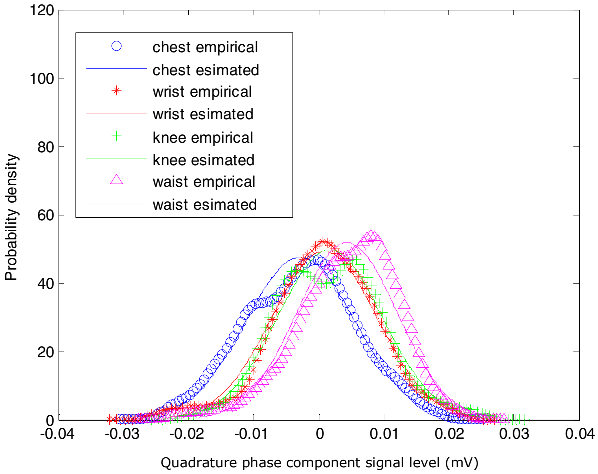

Fig. 5 Empirical and estimated probability densities of the quadrature component for a selection of antenna positions in the reverberation chamber.

IV. COMPLEX AUTOCORRELATION

Due to the positioning of nodes in BANs and physiological and biomechanical movements of the human body, it is anticipated that BAN channels will be subject to anisotropic signal transmission and reception. A PDF that can be used to model fading scenarios in which AOD or AOA of multipath waves is either isotropic or non-isotropic is the Von Mises distribution [12]. Letting θ represent θ_R or θ_T as required, the Von Mises PDF for the angle of departure (or arrival) distribution of the scattered signal contribution, $f_\Theta(\theta)$, is given by [12]

$$f_\Theta(\theta) = \frac{\exp\left[\kappa\cos\left(\theta-\theta_p\right)\right]}{2\pi I_0(\kappa)}, \qquad \theta\in[-\pi,\pi) \tag{4}$$

where $I_0(\bullet)$ is a modified Bessel function of the first kind order zero, $\kappa \geq 0$, where κ can represent κ_T or κ_R as required, controls the width of the AOD or AOA of scatter components and θ_p accounts for the mean direction of departure or arrival distributed on $[-\pi,\pi)$. When $\kappa = 0$, (4) reduces to the uniform distribution and the fading experienced by the receiver is due to isotropic scattering. When κ becomes larger, the AOD or AOA becomes increasingly unidirectional with $\kappa \to \infty$ describing deterministic scattering.

Letting $E[\bullet]$ denote the mathematical expectation operator, the autocorrelation of a wide sense stationary complex process may be written as

$$\phi_{zz}(\tau) = E\left[z(t)z^*(t+\tau)\right] \tag{5}$$

where $z^*(t)$ is the complex conjugate of $z(t)$. Using (2) as a model for the complex received signal and assuming that θ_R and θ_T are independent random variables, the expectation in (5) normalized to $\sqrt{\Omega}$ for non-isotropic scattering conditions has been found as (6) [7, p.66] where $\tilde{\phi}_{zz}(\tau)$ represents the normalized ACF.

Table II shows the parameter estimates for equation (6) obtained from the normalized empirical autocorrelation function. The empirical ACF was calculated for 400 sample lags (i.e. a continuous duration of 2 seconds) selected from the measured data. The parameter estimates were obtained using a non-linear optimization algorithm in MATLAB. What is immediately obvious from Table II is that the parameter estimates for κ_R are always greater than zero even for the reverberation chamber showing that signal reception in dynamic body area networks will be non-isotropic. Over both environments, the values of κ_R and κ_T tended to be largest for positions closest to the transmit antenna such as the chest and waist. For antennas positioned on the highly dynamic positions on the body such as the ankle, knee and wrist the spread of the AOA was greatest. The perceived spread of the AOD of the complex signal was generally observed to be lowest for the anechoic chamber with the increased multipath in the reverberation chamber reducing the size of κ_T.

Fig. 6 shows a selection of the real part of the complex autocorrelation function of (6) fitted to the empirical autocorrelation functions for the waist and wrist in the anechoic chamber. As we can see even over this considerable time span the model provided in equation (6) provides a good fit to the data. Overall, these are representative of the type of fits achieved. Fig. 7 shows the real part of (6) fitted to the empirical ACF for the ankle positioned antenna in the reverberation chamber. Also shown for comparison is the well-known autocorrelation model associated with Clarke's signal reception model [13], $\tilde{\phi}_{zz}(\tau) = J_0\left(2\pi f_m^R \tau\right)$ where J_0 is a zero-order Bessel function of the first kind. As we can see, in reverberant environments, the motion of the transmitting and receiving antennas in BANs mean that the real part of the complex ACF decays slightly quicker in BAN channels than traditional land mobile channels. Although not shown due to space limitations, it was observed from the results that because BAN channels are quite often subject to non-isotropic signal transmission, the cross-correlation between the in-phase and quadrature components is nonzero.

$$\tilde{\phi}_{zz}(\tau) = \frac{1}{K+1}\frac{I_0\left(\sqrt{\kappa_T^2 - 4\pi^2\left(f_m^T\right)^2\tau^2 + j4\pi\kappa_T\cos\left(\theta_p^T\right)f_m^T\tau}\right)}{I_0(\kappa_T)} \times \frac{I_0\left(\sqrt{\kappa_R^2 - 4\pi^2\left(f_m^R\right)^2\tau^2 + j4\pi\kappa_R\cos\left(\theta_p^R\right)f_m^R\tau}\right)}{I_0(\kappa_R)}$$
$$+\frac{K}{K+1}\exp\left[-j\left(2\pi f_m^T\tau\cos\left(\pi-\theta_d\right) + 2\pi f_m^R\tau\cos\left(\theta_d\right)\right)\right] \tag{6}$$

TABLE II

PARAMETER ESTIMATES FOR ALL ON-BODY CHANNELS OVER BOTH ENVIRONMENTS (UNITS OF ALL DOPPLER FREQUENCIES ARE HZ & ANGLES ARE RADIANS)

	Anechoic Chamber								Reverberation Chamber							
Posn	K	f_m^R	f_m^T	θ_p^R	θ_p^T	θ_d	κ_R	κ_T	K	f_m^R	f_m^T	θ_p^R	θ_p^T	θ_d	κ_R	κ_T
Ankle	0.05	12.80	9.06	0.77	−3.14	1.57	2.94	37.02	0.05	6.20	4.81	1.08	3.14	−2.57	5.94	1.39
Chest	0.26	41.05	41.18	0.00	3.13	0.48	192.71	78.68	0.09	13.28	12.08	−3.13	0.00	1.34	1.98	36.40
Elbow	0.17	8.73	8.93	0.00	−2.72	−1.73	5.69	5.57	0.22	7.66	7.79	0.00	3.14	1.22	6.39	3.48
Head	0.25	4.35	3.62	0.56	−3.14	1.55	4.33	2.47	0.05	48.92	50.00	−3.14	0.26	1.29	131.90	55.67
Knee	0.09	10.70	8.83	0.43	−3.14	1.56	2.15	9.31	0.14	10.62	10.74	0.00	2.75	0.97	4.35	7.99
Waist	0.24	13.56	13.43	0.00	−3.13	−0.20	27.00	60.18	0.17	30.65	31.47	0.00	2.84	−1.60	11.39	29.40
Wrist	0.15	9.35	7.44	−0.79	−3.11	0.00	3.27	24.79	0.04	23.92	20.15	0.49	3.14	2.10	3.24	6.51

V. CONCLUSIONS

In this paper we have investigated the characteristics of the complex received signal in body area networks for two environments at the opposite ends of the multipath spectrum. For anechoic conditions it has been found that the assumption of Gaussian distributed quadrature components as commonly assumed in popular fading models may not always be appropriate. For highly reverberant environments, the additional multipath generated by the local surroundings will mean this assumption may be judiciously applied. Overall the power imbalance between the quadrature components in BAN channels was found to be low. For the first time a non-isotropic model with an optional dominant signal component was considered for the complex received signal in BANs. This model was used with the temporal autocorrelation function derived for mobile-to-mobile communications [7] to model the autocorrelation of complex signal reception in BANs.

ACKNOWLEDGMENTS

This work was supported by the U.K. Royal Academy of Engineering and the Engineering and Physical Research Council (EPSRC) under Grant Reference EP/H044191/1 and by the Leverhulme Trust, UK through a Philip Leverhulme Prize.

REFERENCES

[1] S. L. Cotton & W. G. Scanlon, "Higher order statistics for lognormal small-scale fading in mobile radio channels," *IEEE Antennas & Wireless Propagation Letters*, vol. no. 6, pp. 540–543, 2007.

[2] Y. I. Nechayev, Z. H. Hu, and P. S. Hall, "Short-term and long-term fading of on-body transmission channels at 2.45 GHz," *Loughborough Antennas & Propagation Conf.*, Loughborough, 2009, pp. 657–660.

[3] M. Kim and J. I. Takada, "Statistical model for 4.5-GHz narrowband on-body propagation channel with specific actions," *IEEE Antennas and Wireless Propagation Letters*, vol. 8, pp. 1250-1254, 2009.

[4] D. B. Smith, *et al.*, "Temporal correlation of dynamic on-body area radio channel," *Elect. Ltrs.*, vol. 45, no. 25, pp. 1212–1213, Nov. 2009.

[5] S. Van Roy, C. Oestges, F. Horlin, P. De Doncker, "A comprehensive channel model for UWB multisensor multiantenna body area networks," *IEEE Trans on Antennas and Prop.*, vol.58, no.1, pp.163-170, Jan. 2010.

[6] S. L. Cotton, G. A. Conway, and W. G. Scanlon, "A time-domain approach to the analysis and modeling of on-body propagation characteristics using synchronized measurements at 2.45 GHz," *IEEE Trans on Antennas and Prop.*, vol. 57, no. 4, pp. 943–955, Apr. 2009.

[7] A. Zajic: Mobile-to-Mobile Wireless Channels, Artech House 2013.

[8] G. A. Conway and W. G. Scanlon, "Antennas for over-body-surface communication at 2.45 GHz," *IEEE Transactions on Antennas and Propagation*, vol.57, no.4, pp.844-855, April 2009.

[9] G. L. Stüber: Principles of Mobile Communication, 3rd Edition, Springer 2011.

[10] A. Abdi, C. Tepedelenlioglu, M. Kaveh and G. Giannakis, "On the estimation of the K parameter for the Rice fading distribution," *IEEE Communications Letters*, vol. 5, no. 3, p. 92-93, March 2001.

[11] A. S. Akki and F. Haber, "A statistical model of mobile-to-mobile land communication channel," *IEEE Transactions on Vehicular Technology*, vol.35, no.1, pp. 2- 7, Feb 1986.

[12] A. Abdi, J. A. Barger and M. Kaveh, "A parametric model for the distribution of the angle of arrival and the associated correlation function and power spectrum at the mobile station," *IEEE Transactions on Vehicular Technology*, vol. 51, no. 3, pp.425-434, May 2002.

[13] R. H. Clarke, "A statistical theory of mobile radio reception," *Bell Systems Tech. Journal*, vol. 47, no. 6, pp. 957–1000, July/August 1968.

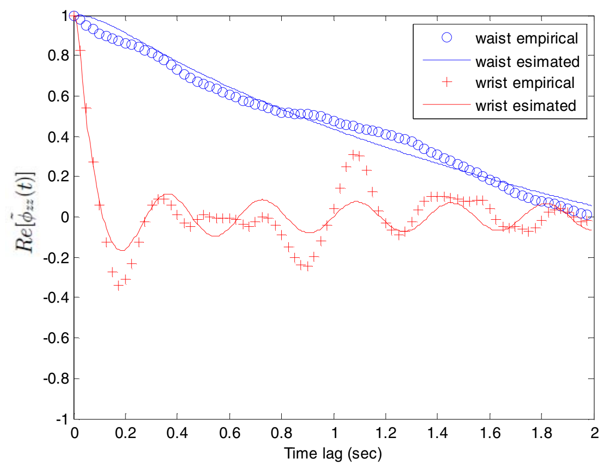

Fig. 6 Real part of the normalized empirical ACF compared to model in (6) for the waist and ankle positioned antennas in the anechoic chamber. All parameter estimates for the theoretical model are given in Table II.

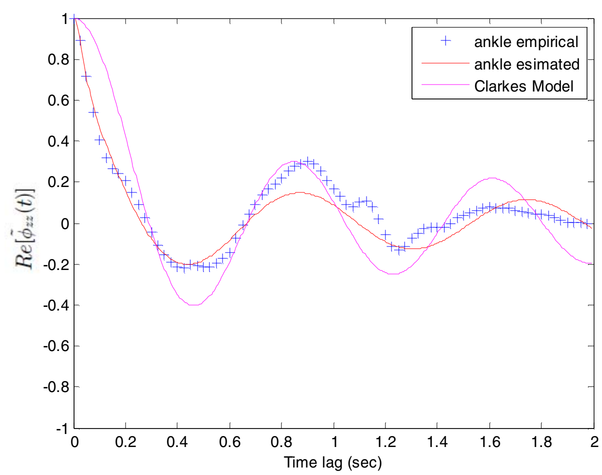

Fig. 7 Real part of the normalized empirical ACF compared to model in (6) for the ankle in the reverberation chamber. All parameter estimates for the theoretical model are given in Table II. f_m^R = 1.3 Hz for Clarke's model.